An Electrically Coupled Network of Skeletal Muscle in Zebrafish Distributes Synaptic Current

Victor M. Luna and Paul Brehm

Department of Neurobiology and Behavior, State University of New York at Stony Brook, Stony Brook, NY 11794

Fast and slow skeletal muscle types are readily distinguished in larval zebrafish on the basis of differences in location and orientation. Additionally, both muscle types are compact, rendering them amenable to in vivo patch clamp study of synaptic function. Slow muscle mediates rhythmic swimming, but it does so purely through synaptic drive, as these cells are unable to generate action potentials. Our patch clamp recordings from muscle pairs of zebrafish reveal a network of electrical coupling in slow muscle that allows sharing of synaptic current within and between segmental boundaries of the tail. The synaptic current exhibits slow kinetics (τ_{decay} ~4 ms), which further facilitates passage through the low pass filter, a consequence of the electrically coupled network. In contrast to slow muscle, fast skeletal muscle generates action potentials to mediate the initial rapid component of the escape response. The combination of very weak electrical coupling and synaptic kinetics (τ_{decay} <1 ms) too fast for the network low pass filter minimizes intercellular sharing of synaptic current in fast muscle. These differences between muscle types provide insights into the physiological role(s) of electrical coupling in skeletal muscle. First, intrasegmental coupling among slow muscle cells allows effective transfer of synaptic currents within tail segments, thereby minimizing differences in synaptic depolarization. Second, a fixed intersegmental delay in synaptic current transit, resulting from the low pass filter properties of the slow muscle network, helps coordinate the rostral–caudal wave of contraction.

The Journal of General Physiology

INTRODUCTION

Intercellular electrical coupling is well documented for both cardiac and smooth muscle types (Saez et al., 2003), but published reports of electrical coupling in skeletal muscle are scarce. In *Xenopus* tadpole tail (Blackshaw and Warner, 1976) and in regenerating salamander limb (Dennis, 1975) the muscle cells are dye coupled and electrically coupled. Electrical coupling has also been reported for embryonic mammalian skeletal muscle both in cell culture (Constantin and Cronier, 2000) and in vivo (Dennis et al., 1981; Schmalbruch, 1982). In *Xenopus* (Armstrong et al., 1983) and mammalian (Dennis et al., 1981) muscle the coupling was eliminated early in animal development. However, in at least one case, electrical coupling was maintained throughout the life of the adult animal (Teravainen, 1971). Lamprey body wall musculature is organized in a way that not all of the muscle fibers receive direct innervation. Therefore, persistent coupling in this animal likely provides a means for distributing the synaptic current from innervated cells.

Recent studies on zebrafish larva have shown that skeletal muscle cells in the tail are dye coupled (Nguyen et al., 1999; Buss and Drapeau, 2000), and paired recordings have indicated occasional sharing of synaptic current (Buss and Drapeau, 2000; Luna et al., 2004). In the present study, we found that slow skeletal muscle, unlike its fast counterpart, exhibited levels of coupling reminiscent of cardiac and smooth muscle types (Saez et al., 2003). This coupling is maintained for at least 1 wk, but it is not known whether it persists in fully developed, adult zebrafish. Our experiments were aimed at determining the physiological role played by this high level of electrical coupling in developing zebrafish. In accordance with a previous proposition (Buss and Drapeau, 2000) we found that coupling was critical to synaptic physiology of slow muscle and to the depolarization that underlies rhythmic swimming. Our findings revealed the importance to slow muscle of sharing synaptic current through an electrically coupled network and point to two important functions served by this network in skeletal muscle. First, it forms a low pass filter similar to certain CNS circuits (Galarreta and Hestrin, 1999; Gibson et al., 1999), which serves to slow transjunctional synaptic current kinetics (Bennett, 1966). This, in turn, promotes both muscle depolarization (Jaramillo et al., 1988) and the ability to transit current to more distal electrical junctions. Second, the network filter imposes a fixed delay in intersegmental synaptic depolarization (Bennett, 1966). The fidelity provided by this filter aids CNS synchronization of the rostral–caudal wave of depolarization that underlies undulatory swimming. Overall, these findings point to a physiological importance of electrical coupling for providing uniform contractions

Correspondence to Paul Brehm: pbrehm@notes.cc.sunysb.edu

Abbreviations used in this paper: EPC, end-plate current; LEC, leading edge current; TTX, tetrodotoxin.

within tail segment as well as timing intersegmental contractions for smooth and rhythmic swimming.

MATERIALS AND METHODS

Experiments were performed on either wild-type (*Danio rerio*, brian strain) or homozygous *relaxed* zebrafish between the ages of 96 to 168 h post-fertilization (Granato et al., 1996; Ono et al., 2001). Immediately before recording, the fish was decapitated, mounted on its side, and the top side skinned to provide access for the patch electrodes. The chamber was then placed on a Carl Zeiss MicroImaging, Inc. FS-1 microscope that was fixed upon an X-Y motorized platform (model MXMS, Siskiyou Design Instruments). Muscle cells were visualized by means of DIC optics using a 40× LD water-immersion physiology objective. To access the deeper fast muscle, the superficial layer of slow muscle was teased away using a patch pipette.

Dual patch clamp recordings were performed using a HEKA EPC-10/2 amplifier (Instrutech) and four-axis motorized manipulators (model MX7600, Siskiyou Designs). Continuous records of synaptic current were digitized at 50 kHz and filtered at 10 kHz before off-line analysis. Measurements of rise time, amplitude, and decay time constants of synaptic currents were performed using MiniAnalysis (Synaptosoft). To obtain time constants, the region of current decay between 10% and 90% were fit by a single exponential curve. Electrodes for whole cell muscle recordings were pulled to an outer diameter of 2–3 μm and lightly fire polished. When filled with intracellular solution for whole cell recording (in mM: 120 KCl, 5 K-HEPES, and 5 K-BAPTA), the resistance corresponded to 3–5 MΩ. Electrodes used for extracellular recordings were pulled to an outer diameter of 6–10 μm. When filled with bath recording solution (in mM: 110 NaCl, 5 Na-HEPES, 4 $CaCl_2$, 3 glucose, 2 KCl. and 1 $MgCl_2$), the resistance corresponded to 0.5–1.5 MΩ. In some cases, the osmolarity of the extracellular pipette solution was further elevated by addition of 50 mM sucrose in order to increase the frequency of spontaneous synaptic events during paired extracellular–intracellular recordings. This extracellular electrode was first used to scan muscle cells for a location of active synapses followed by application of mild suction to improve the signal-to-noise ratio.

To record evoked synaptic currents associated with fictive swimming, homozygous paralytic *relaxed* fish were used. In this case, however, the fish were not decapitated and tetrodotoxin was not present in the bath recording solution. Fictive swimming was elicited by transiently shining a flashlight at either eye of the fish (Ritter et al., 2001; Buss and Drapeau, 2001, 2002; Luna et al., 2004; Masino and Fetcho, 2005). Tetrodotoxin (Alomone Labs) was stored at 300 μM in 0.1-ml aliquots at −20°C. The gap junction blocker 18β-glycyrrhetinic acid (Sigma-Aldrich) was stored as a 0.1 M stock solution in DMSO at room temperature. All data is presented as mean ± standard deviation.

RESULTS

Muscle Cells Form an Electrically Coupled Network with Low Pass Filter Characteristics

Dual voltage clamp recordings were performed on adjacent slow–slow, fast–fast, and slow–fast skeletal muscle pairs. The slow and fast muscle types were distinguished on the basis of position and orientation. Slow type comprises the superficial layer of horizontal muscle, and deeper fast muscle layers are diagonally oriented with the respect to the long axis of the tail (van Raamsdonk et al., 1978, 1982; Buss and Drapeau, 2000; Luna et al., 2004). To determine the extent of electrical coupling, sine wave command pulses (±10 mV) of varying frequencies were applied to one cell of the pair while the membrane potential of the second cell was held constant at −90 mV (Fig. 1 A). At frequencies between 1 Hz and 6 kHz the coupling coefficients were determined by the ratio of follower cell current to command cell current. No evidence of electrical coupling was observed in any of the four mixed slow–fast muscle pairs tested. By contrast, all 30 slow–slow pairs that were tested showed bidirectional electrical coupling. At 1 Hz, the coupling coefficients ranged from 0.4 to 0.7 with a mean of 0.6 ± 0.1 ($n = 6$). The coefficient exhibited a steep dependence on sine wave frequency, and the functional coupling approached zero at frequencies near 2 kHz (Fig. 1 D). Fast muscle was less effectively coupled than slow muscle at all frequencies tested, and 8 of the 26 cell pairs tested showed no measurable coupling. In those fast muscle pairs that exhibited measurable coupling, the coefficients at 1 Hz averaged 0.1 ± 0.1 ($n = 6$; Fig. 1 D). The differences in coupling were also evident in the attenuation of transjunctional spontaneous synaptic currents (Fig. 1 B).

The dependence of coupling coefficients on signal frequency is a central property of the muscle network's low pass filter. The time constants that determine the filter characteristics are determined by the resistive and capacitive properties of the muscle (Bennett, 1966). In addition to attenuating the signals, the low-pass filtering imposes a phase lag that is frequency dependent (Fig. 1 A). Because the slow and fast muscle cells have similar low pass filter characteristics, this phase lag is similar for fast–fast and slow–slow muscle pairs.

Slow and fast muscle were separately tested for dye coupling at 5 min after establishing the whole cell recording configuration. The electrode was filled with intracellular recording solution containing 0.1% Lucifer yellow (Fig. 1 C). Under these conditions, the dye spread to 1 ± 1 ($n = 18$) fast muscle cells compared with 13 ± 6 ($n = 13$) for slow muscle cells. In both muscle types, the dye spread in a cellular pattern that was intra- and intersegmental.

Recordings from slow muscle pairs were next compared for differences in intra- and intersegmental electrical coupling (Fig. 1 E). Comparisons of coupling coefficients over the range of frequencies between 1 and 6 kHz revealed no significant differences between intra- and intersegmental coupling in slow muscle. This symmetry in electrical coupling agrees with the symmetrical spread of injected dye into slow muscle (Fig. 1 C) (Nguyen et al., 1999; Buss and Drapeau, 2000).

Neuromuscular Synaptic Currents Differ in Fast and Slow Muscle

In addition to providing quantitative estimates of network electrical coupling, the paired muscle recordings

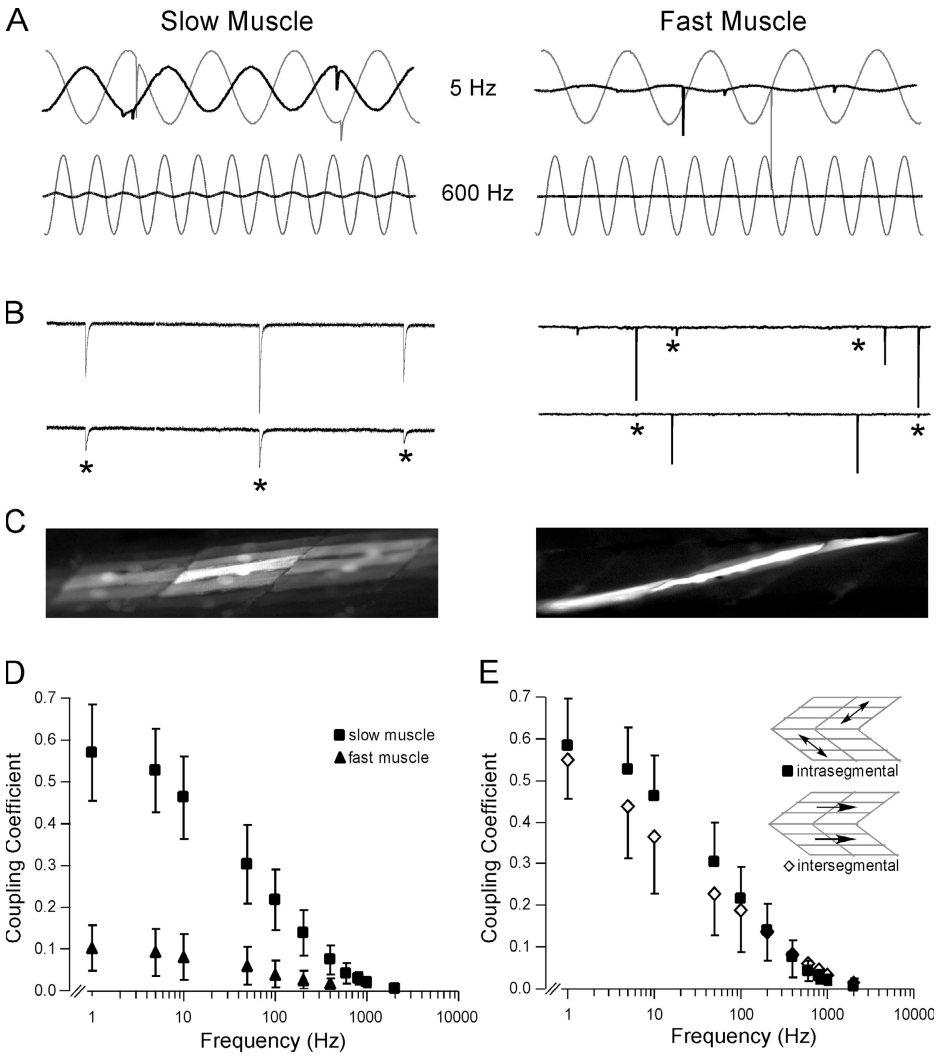

Figure 1. Electrical coupling in slow and fast skeletal muscle. (A) Sinusoidal command potentials (±10 mV centered on −90 mV) of varying frequencies were injected into slow muscle (left) and fast muscle (right) pairs. Examples of membrane currents in the injected (gray trace) and the follower (black trace) cell in response to 5 and 600 Hz command sine waves. (B) Sample traces of spontaneous mEPCs and their transjunctional counterparts (asterisk) in paired slow (left) and paired fast (right) muscle. (C) Images of dye spread in slow (left) and fast (right) muscle. Images were taken ~5 min after establishing a whole cell configuration with 0.1% Lucifer yellow in the patch pipette. In this particular example of fast muscle, the dye spread to both inter- and intrasegmental neighboring cells. However, the intrasegmental cells are difficult to discern because they are much dimmer. (D) Sine wave frequency versus mean coupling coefficient for six slow and six fast muscle pairs. Mean coupling coefficients were determined at each frequency as the ratio of follower current to command cell current. (E) Comparison of mean intrasegmental (square; $n = 6$) and intersegmental (diamonds; $n = 5$) coupling coefficients for slow muscle pairs. All recordings were performed in 1.5 μM TTX.

revealed the electrotonic transfer of spontaneous synaptic currents between cells (Fig. 1 B). To ensure that the synaptic currents were spontaneous and not evoked, 1.5 μM tetrodotoxin (TTX) was routinely added to the recording solution. Analysis of both muscle types revealed two functionally distinct classes of spontaneous synaptic currents (Fig. 2 A). A primary type is characterized by fast rise, fast decay, and large amplitude events while a secondary type bears a slightly slower rise, much slower decay, and much smaller amplitude. In scatter plots of individual event 10–90% rise time versus decay time constants, two separate clouds of points could be distinguished (Fig. 2 B). The secondary events were highly variable in both rise and decay times but the kinetics of the primary events were so consistent that the points formed a very tight cloud. Separation of primary and secondary events was also reflected in scatter plots of both event amplitude versus 10–90% rise time (Fig. 2 C) and amplitude versus decay time constant (not depicted).

Slow and fast muscle types exhibited both classes of current. However, the kinetics of each type differed between muscle types. In fast muscle, the primary synaptic currents faithfully decay along a single exponential time course with a mean time constant of 0.75 ± 0.25 ms ($n = 20$; Fig. 2; Table I). By contrast, the decay of primary synaptic currents in slow muscle is much slower and variable, with many of the currents deviating from an exponential time course. Some events required fit by the sum of two exponential curves while others show complicated time courses that cannot be well fit by the sum of exponentials. However, to compare the time constants to fast muscle, the primary events were force fit to a single exponential function yielding values of 3.93 ± 1.61 ms ($n = 18$ cells; Table I). By this method of quantitation, the decay time constant of primary synaptic current was fivefold slower in slow muscle than fast muscle. In contrast, 10–90% rise time of the primary kinetic class was similar for slow (0.33 ± 0.13 ms) and fast (0.26 ± 0.04 ms) muscle (Table I).

The secondary currents of slow and fast muscle were also distinct. In slow muscle, the secondary class averaged 51 ± 20 pA compared with 35 ± 12 pA for fast

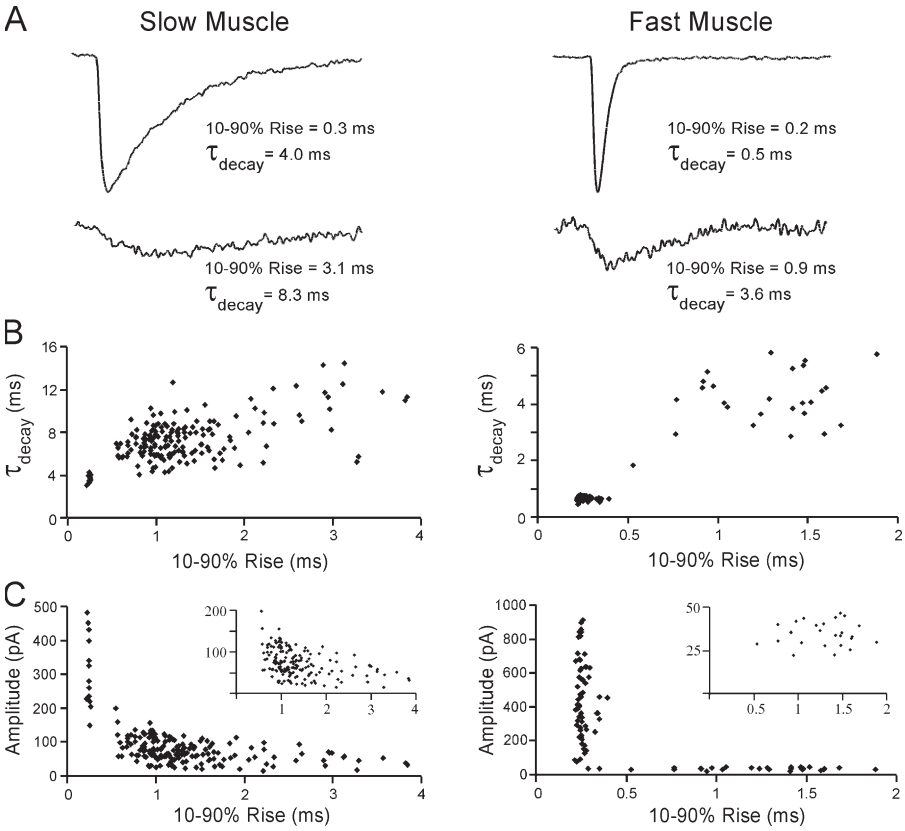

Figure 2. Two classes of spontaneous mEPCs in slow and fast skeletal muscle. (A) Sample primary (top) and secondary (bottom) spontaneous synaptic currents recorded in a single slow (left) and fast (right) muscle cell (Vm = −90 mV). (B) Scatter plot of event 10–90% rise time versus τ_{decay} for a single slow (left) and a fast (right) muscle cell. (C) The scatter plots 10–90% rise time versus amplitude for a single slow (left) and a fast (right) muscle cell. Insets are expanded plots of secondary mEPC cloud of events. All recordings were performed in 1.5 μM TTX.

muscle (Table I). The rise times of secondary synaptic currents averaged 2.29 ± 0.88 ms in slow muscle and 1.01 ± 0.25 ms in fast muscle (Table I). The mean time constants of decay spanned 3.51 to 12.94 ms (8.00 ± 2.69 ms) for slow muscle compared with 1.58 to 4.44 ms (2.85 ± 0.90 ms) for fast muscle (Table I).

Differences in Primary Current Kinetics between Slow and Fast Muscle Are Not a Consequence of Poor Voltage Control Caused By Electrical Coupling

The presence of strong electrical coupling between slow muscle cells potentially compromises the quality of the voltage control in our recordings and may lead to distortion of synaptic current waveforms. Thus, it becomes important to determine the extent to which differences in synaptic waveform between fast and slow muscle reflect voltage clamp distortion. The authentic time course of synaptic currents was determined by recording the extracellular field current (Fig. 3 A). This method provides localized recording of synaptic currents from individual synapses and the time course is limited only by the bandwidth of the electronics (Fatt and Katz, 1952; Wernig, 1976; Van der Kloot and Naves, 1996). Using this approach, it was possible to pair some extracellular recordings with their intracellular voltage clamp counterparts (Fig. 3 A). Comparisons of rise and decay by these two methods provided an index of distortion under whole cell recording (Fig. 3 B; Table II). The rising phases of the intracellularly recorded spontaneous synaptic currents were distorted due to the very fast kinetics (Fig. 3, A and B). In fast muscle, the distortion associated with electrical coupling was less due to the very weak coupling coefficients. However, the kinetics of synaptic current was much faster in this muscle type so the distortion due to the limitations of whole cell patch clamp was greater. The extent of the distortion was reflected in scatterplots of kinetics comparing the intracellular versus extracellular counterparts (Fig. 3 B). Both rise times and decay times were extended in the intracellular recordings of mEPCs (Fig. 3 B).

TABLE I

Miniature End-plate Current Kinetics

	Primary Class			Secondary Class		
Muscle Type	Rise (ms)	τ_{decay} (ms)	Amp (pA)	Rise (ms)	τ_{decay} (ms)	Amp (pA)
Slow (n = 18)	0.33 ± 0.13	3.93 ± 1.61	302 ± 171	2.29 ± 0.88	8.00 ± 2.69	51 ± 20
Fast (n = 20)	0.26 ± 0.04	0.75 ± 0.25	369 ± 130	1.01 ± 0.25	2.85 ± 0.90	35 ± 12

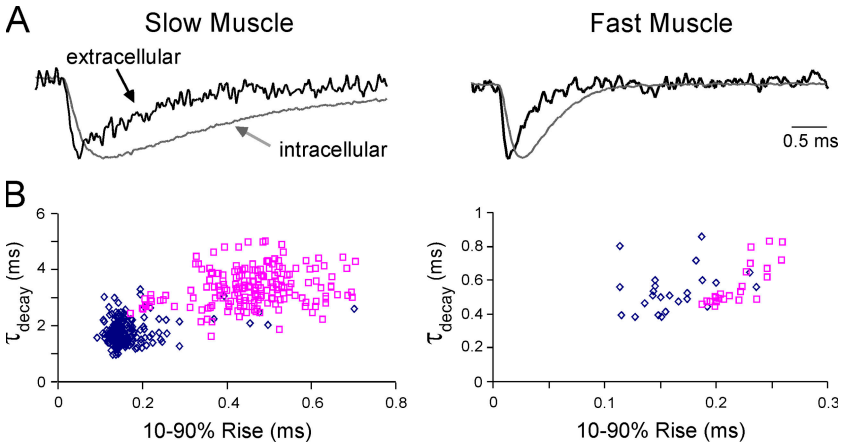

Figure 3. Paired intracellular–extracellular recordings of mEPCs as an index of distortion. (A) Sample slow muscle (left) and fast muscle (right) mEPCs (gray trace) recorded at −90 mV along with their extracellular counterpart (black trace). (B) Scatterplots of decay versus 10–90% rise time for extracellularly recorded spontaneous synaptic events (blue) and their intracellular counterpart (pink).

The quantitative indices for distortion were determined on the basis of the ratios of intracellular/extracellular current rise from 10 to 90% peak amplitude (Table II). The mean rise time distortion index was 2.06 ± 0.53 (n = 5) for slow muscle and 2.26 ± 0.53 (n = 5) for fast muscle. The decay distortion index, determined by the ratio of intracellular/extracellular fits to single exponential curves was 1.61 ± 0.32 for slow muscle and 1.75 ± 0.38 for fast muscle (Table II). In addition to providing the real time course of synaptic current, these extracellular recordings validated the differences in kinetics between slow and fast muscle.

The Secondary Current Class Represents Transjunctional Reflections of Primary Spontaneous Synaptic Currents

Several lines of evidence show that the secondary class of small synaptic currents in slow and fast muscle represent electrotonic reflections of primary synaptic currents from neighboring muscle cells and not a directly generated class of events. First, the slow events were never observed in extracellular recordings, consistent with transcellular passage (Fig. 4 A). All of the paired intracellular and extracellular events represented primary synaptic currents on the basis of kinetics and amplitude. Second, recordings from both muscle types show that application of 100 μM 18β-glycerrhetinic acid (18βGA) (Davidson et al., 1986; Davidson and Baumgarten, 1988; Goldberg et al., 1996; Proulx et al., 1997) to block electrical coupling results in the total disappearance of this secondary current class in slow muscle recordings (n = 5) (Fig. 4 C). Similarly, in all five slow muscle cells tested, treatment with 18βGA effectively blocks dye coupling (Fig. 4 B). Third, primary currents recorded in one cell occasionally show electrotonic reflections in a neighboring cell (Fig. 1 B). Primary and secondary currents are considered paired only when peak current amplitudes occur within <5 ms of each other. The low frequency of spontaneous events greatly reduces the risk of errant pairing. The occurrence of synaptic pairs is infrequent in fast muscle but is commonly observed in slow muscle.

The difference in coupling coefficients, as well as differences in secondary current class rise times (Fig. 2), between fast and slow muscle suggests that the extent of synaptic sharing differs between muscle type networks. Approaches such as the use of dye coupling or sine wave current injections will not determine the extent to which functional sharing of synaptic currents can occur. To address the extent of the functional networks in these two different muscle types, we turned to paired recordings. Through the combined use of attenuation (amplitude ratios), kinetic distortion, and phase delays, it is possible to trace the origins of synaptic currents using paired recordings (Figs. 5 and 6). The data in Fig. 5 illustrates a representative pair of fast muscle cells. Plots of amplitude ratios from the perspective of one arbitrary cell in all recordings revealed at least one cluster of points. In most recordings, one cluster had fractional values <<1 and a second cluster had fractional values >>1 (Fig. 5 D). These reciprocal clouds represent events that were likely generated in one of the paired cells as the larger of the two events displayed the fast kinetics characteristic of primary currents. The smaller of each pair showed slow kinetics and amplitudes

TABLE II

Paired Extracellular–Intracellular Recording

	Extracellular		Intracellular		Distortion (Intra/Extra)	
Muscle Type	Rise (ms)	τ_{decay} (ms)	Rise (ms)	τ_{decay} (ms)	Rise	Decay
Slow (n = 5)	0.21 ± 0.06	1.95 ± 0.51	0.38 ± 0.11	2.95 ± 0.78	2.06 ± 0.53	1.61 ± 0.32
Fast (n = 5)	0.12 ± 0.02	0.38 ± 0.07	0.24 ± 0.04	0.64 ± 0.14	2.26 ± 0.53	1.75 ± 0.38

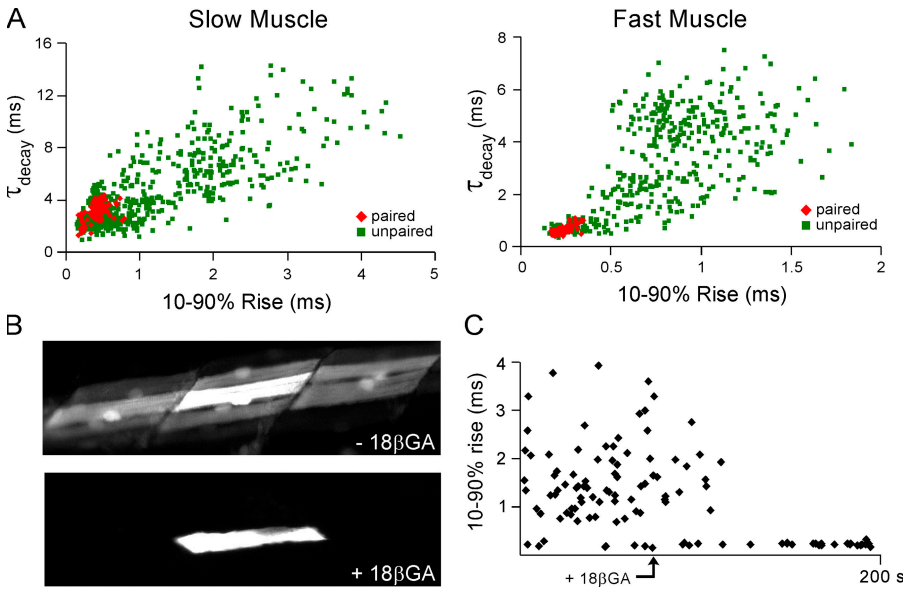

Figure 4. The secondary mEPC class represents electrotonic reflections through electrical junctions. (A) Scatterplots of 10–90% rise time versus τ_{decay} for intracellular events with extracellular counterparts (red symbol) and without extracellular counterparts (green symbol). (B) Images of slow muscle dye coupling in the absence (top) and presence (bottom) of 100 μM 18βGA. Images were taken ~5 min after establishing a whole cell configuration with 0.1% Lucifer yellow in the patch pipette. (C) 10–90% rise time versus time of occurrence of mEPCs for a representative slow muscle cell. 100 μM 18βGA was applied near the 60-s marker (indicated by an arrow). All recordings were performed in 1.5 μM TTX.

consistent with those of the secondary class of events (Fig. 5, A and C; Table III). Further tracing of the origins of the two events comes from measurements of phase delay. The event class with amplitude ratios >>1 exhibited a positive delay while the class with ratios <<1 exhibited a negative delay (Fig. 5 D). This reciprocal phase delay was expected on the basis of low pass filtering effects upon transjunctional passage.

A third event cloud with amplitude ratios of ~1 was frequently observed as well (Fig. 5 D). Both synaptic currents showed slow kinetics and small amplitudes that were characteristic of the secondary event class (Fig. 5 B). Unlike the other two clouds, this cloud of events was centered on 0 phase delay (Fig. 5 D). The similarity in attenuation, transformation, and absence of phase delay would be expected if the events were generated in a cell common to the pair.

Synaptic Currents Transit Multiple Electrical Junction Boundaries in Slow Muscle

Because the slow muscle is so effectively coupled, it is likely that synaptic currents can traverse more cell boundaries than fast muscle counterparts. The evidence for this idea comes from measurements of attenuation, kinetics and phase delays. Comparison of the amplitude ratio versus phase delay from slow muscle (Fig. 6 D) to that of fast muscle (Fig. 5 D) reveals two additional clouds of points (x and + clouds) in slow muscle. Both clouds show amplitude ratios that are intermediate to ~1 and either <<1 or >>1 (Fig. 6 D). The intermediate amplitude ratios reflect the reduction in relative attenuation that occurs during a second transjunctional passage. This is a consequence of the slowed kinetics due to the initial transjunctional passage. The negative and positive phase times for each of these classes were also consistent with synaptic currents that were initiated in cells that directly contacted only one of the pair. The difference in kinetics also support this pattern. Unlike ~1 class, where the kinetics are similar in both cells (Fig. 6 B), these currents show distinct rise time differences (Fig. 6 C). Thus, the faster rising current likely transited one slow cell, and the slower rising counterpart likely transited an additional electrical boundary formed by the union of the paired cells (Fig. 6 C).

These measurements of amplitude ratios and phase delays indicate that spontaneous synaptic currents can traverse two slow muscle cells. Patch clamp recordings indicate that coupling is symmetrical, permitting both intrasegmental and intersegmental spread of current. This symmetry suggests that the functional unit surrounding a single slow muscle is composed of 12 cells (Fig. 7 D). As an independent test of the size of the functional network, the total loss of spontaneous current to the network was determined in two ways.

TABLE III

Paired Muscle Recording

	Primary class		First Transcellular Passage		Transformation Index (First passage/ Primary class)	
Muscle Type	Rise (ms)	τ_{decay} (ms)	Rise (ms)	τ_{decay} (ms)	Rise	Decay
Slow (n = 11)	0.27 ± 0.05	4.00 ± 0.36	1.55 ± 0.44	6.76 ± 1.41	5.76 ± 2.27	1.66 ± 0.22
Fast (n = 12)	0.28 ± 0.04	0.89 ± 0.19	0.87 ± 0.27	2.14 ± 0.89	3.23 ± 0.99	2.41 ± 0.87

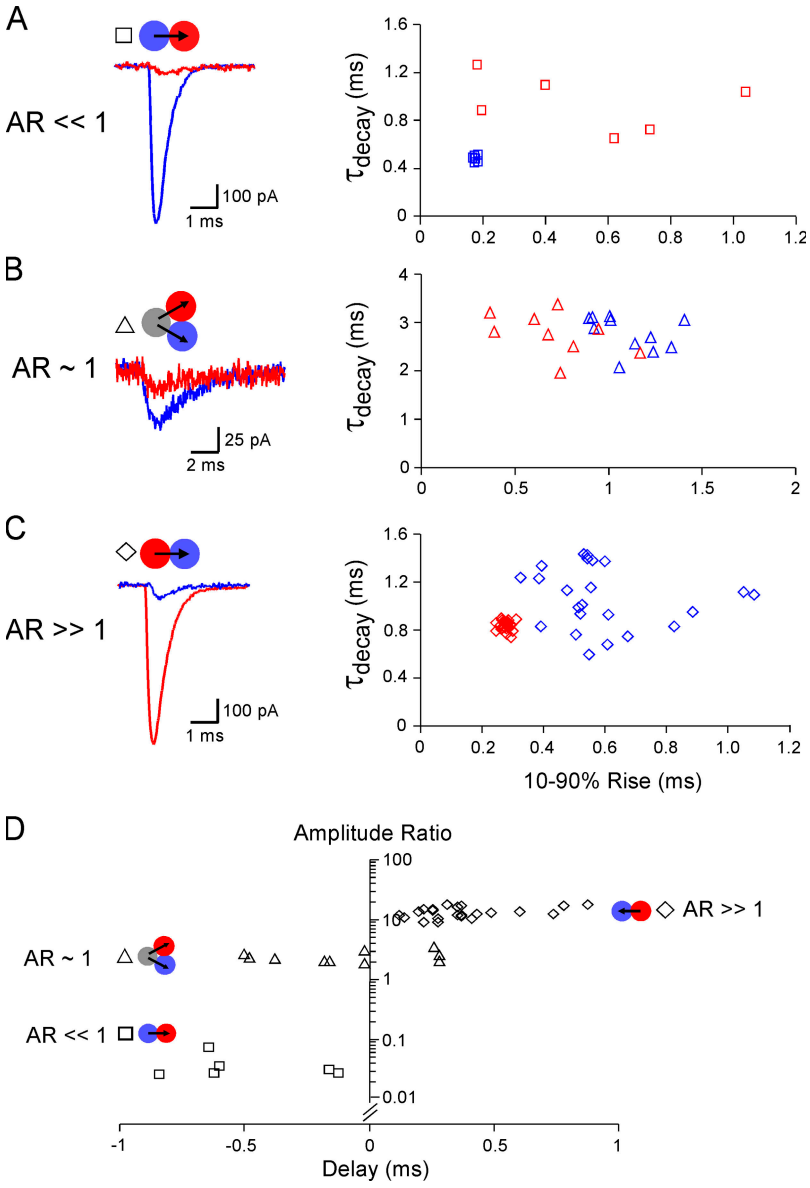

Figure 5. Transformation of mEPCs indicates that the fast muscle network consists of single transjunctional passage. (A–C) Examples of paired mEPCs recorded from two fast muscle cells designated as red and blue. Current traces and scatter plots are color coded according to the cell in which the events were recorded. The amplitude ratios (red cell/blue cell) correspond to $<<1$ (squares), ~ 1 (triangles), and $>>1$ (diamonds). The accompanying scatter plots of 10–90% rise time versus τ_{decay} indicate that the larger of the two events in A and C have the fast kinetics of primary currents, and the smaller of the pair reflects secondary current kinetics. The mEPC pairs in B show mixed slow kinetics, indicating they both likely represent secondary currents. (D) The plot of phase delay versus amplitude ratios show three clouds further pointing to origins of the different amplitude ratios. Currents with amplitude ratios $<<1$ (squares) have negative phase delays; amplitude ratios $>>1$ (diamonds) have positive phase delays; amplitude ratios near unity (triangles) have phase delays centered near zero. All recordings were performed in 1.5 μM TTX.

First, the increase in average maximum peak amplitude of primary synaptic events in slow muscle following 18βGA treatment was measured (Fig. 7 A). This magnitude increase reflects the average current lost to the surrounding electrically coupled network sink. 18βGA treatment is not directly altering primary synaptic current amplitude as it has no effects on fast muscle (Fig. 7 A). For each of the five slow muscle cells tested, the average magnitude of the largest primary spontaneous currents was determined before and after block of electrical coupling. Then the difference current was divided by the average amplitude of the secondary current class, providing an estimate of size of functionally coupled network (Fig. 7 B). The mean estimated value of 10 ± 4 ($n = 5$) for slow muscle supported a functional unit formed by passage through two cells as compared with -2 ± 2 ($n = 5$) for fast muscle.

A second means of estimating the size of the functionally coupled network used the frequency of primary and secondary events. For each of 17 slow and 18 fast muscle cell recordings, we determined the frequency of primary versus secondary events. The frequency of primary events represented the spontaneous synaptic activity generated directly in a muscle cell, whereas the secondary frequency reflected the total amount of transjunctional currents. Dividing the secondary frequency by the primary frequency provided an estimate of the number of functionally coupled cells. The results of this analysis are shown in Fig. 7 C and indicate an average 13 ± 8 cells for slow muscle and 2 ± 2 cells for fast muscle.

All of the measurements of functional coupling point to a functional network of 12 surrounding slow muscle cells. Because coupling is symmetrical within and between segments, the predicted pattern is shown in

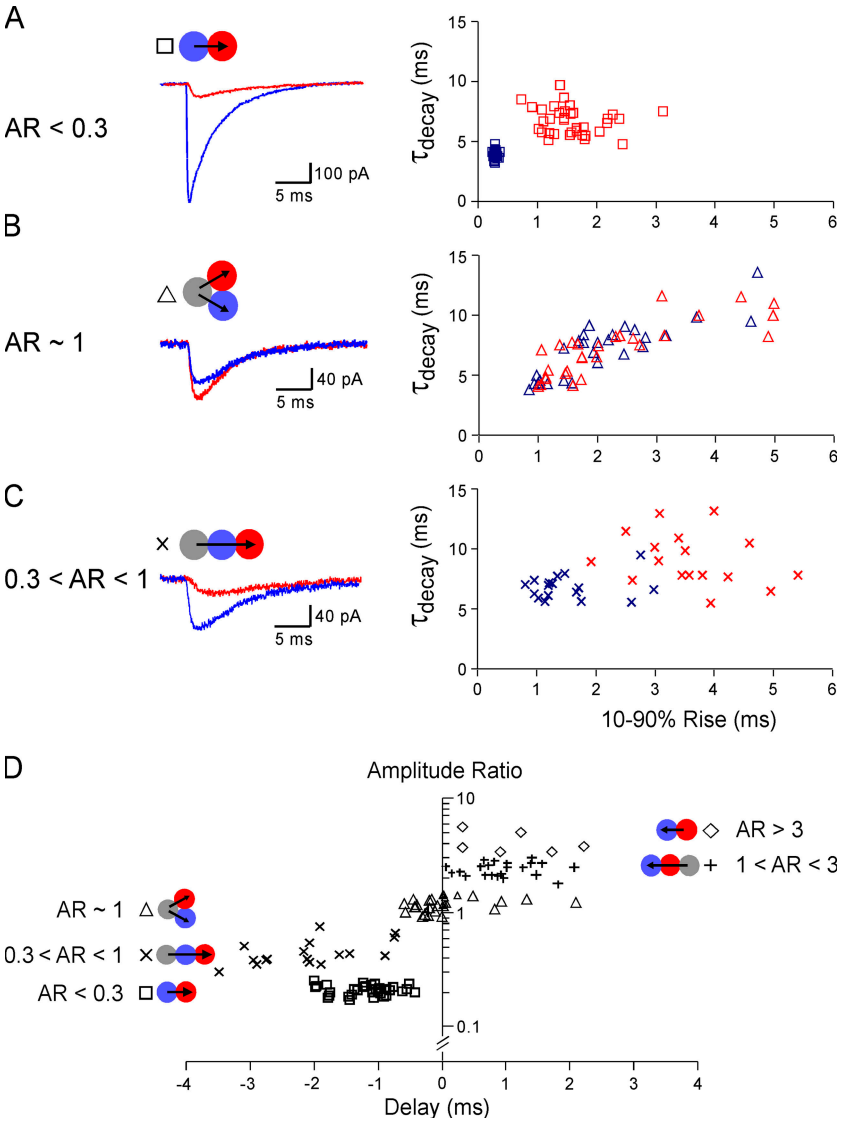

Figure 6. Transformation of mEPCs indicates that slow muscle network consists of two transjunctional passages. (A–C) Examples of paired mEPCs from slow muscle pairs designated as red and blue. The mEPC examples in A and B have amplitude ratios and kinetics that indicate passage through a single transjunctional similar those for fast muscle (see Fig. 5, A and B). (D) Amplitude ratio versus phase delay indicate five clusters of points. Three clusters (diamonds, triangles, and squares) are similar to those shown for fast muscle in Fig. 5. However two additional clusters (+'s and x's) likely represent two junctional passages based on the differences in rise time kinetics shown in C and the intermediate amplitude ratios plotted in D. All recordings were performed in 1.5 μM TTX.

Fig. 7 D. This predicted pattern is very similar to distribution based on dye coupling (Fig. 1 C and Fig. 4 B; see also Nguyen et al., 1999; Buss and Drapeau, 2000).

Evoked Synaptic Currents Reveal a Functional Role of the Electrical Network for Swimming

This 12+1 pattern only applies under conditions wherein a single slow muscle cell serves as a source. Such is the case for spontaneous synaptic currents. However, during evoked responses, many of the muscle cells within a segment represent source cells due to near simultaneous activation. Thus, evoked end-plate currents (EPC) are governed by different source-sink relations than spontaneous synaptic currents. Specifically, muscle cells within an active segment are subject to both gain and loss of electrotonic currents within the network unit and the net loss or gain will be determined by the differences in EPC drive between active cells. To examine directly the quantitative sharing of evoked electrotonic currents, the EPCs in muscle pairs were recorded in the absence and presence of 18βGA. To generate EPCs, the motor neurons were induced to fire action potentials by photoactivation of the visual system. All subsequent experiments were performed in the absence of tetrodotoxin. Light-driven fictive swimming patterns mimic the rhythmic drive that occurs during normal swimming (Buss and Drapeau, 2001, 2002; Ritter et al., 2001; Luna et al., 2004; Masino and Fetcho, 2005). The consequences of this patterned neuronal output in muscle was directly recorded using whole cell muscle clamp (Fig. 8). To eliminate the difficulties associated with contraction, most of the recordings were performed in a mutant line, *relaxed*, which exhibited normal synaptic physiology but failed to contract due to inability to release calcium (Ono et al., 2001; Schredelseker et al., 2005; Zhou et al., 2006).

Recordings of patterned output from slow muscle revealed bouts of beat and glide movements (Buss and

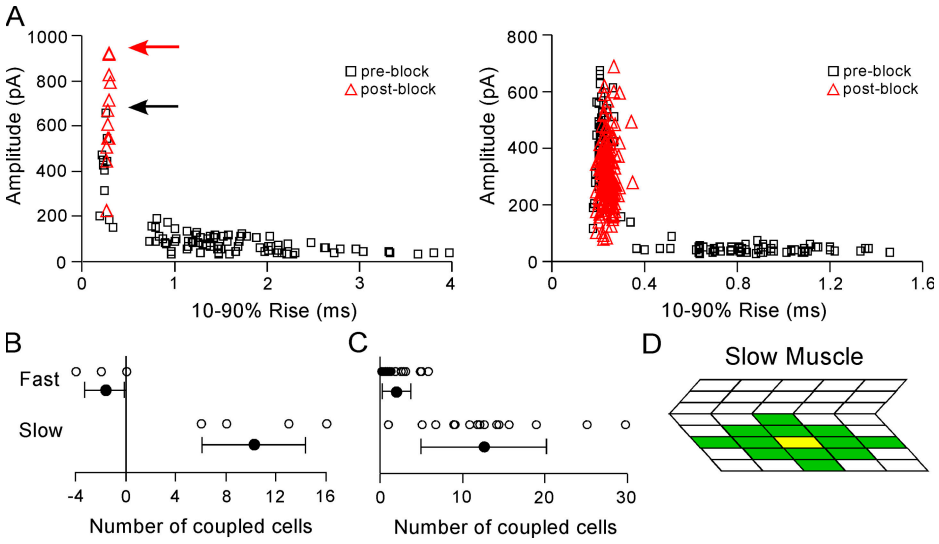

Figure 7. 18βGA block as an estimate of the size of the muscle network. (A) Scatterplot of mEPCs from a slow (left) and fast (right) muscle cell recorded before (black squares) and after (red triangles) application of 100 μM 18βGA. (B) Estimates of the number of functionally coupled neighboring muscle cells on the basis of delta amplitude of primary/mean amplitude of secondary mEPCs. (C) Estimates of the number of electrically coupled neighboring muscle cells recorded on the basis of frequency of secondary/frequency of primary mEPCs. (D) Diagrammatic representation of the predicted distribution of electrically coupled slow muscle cells (in green) that surround a single source cell (in yellow). All recordings were performed in 1.5 μM TTX.

Drapeau, 2001, 2002). In Fig. 8 A, five beat segments with intervening inactive segments are shown. Each beat segment represented a series of four to six rhythmic contractions that propagated caudally along the tail (Fig. 8 B). The electrical counterpart to each segment contraction was composed of sequential compound synaptic currents that summed to produce a plateau inward current lasting, on average, 11.8 ± 2.1 ms ($n = 7$; Fig. 8 B). The intervening interval between these plateau currents averaged 31.4 ± 2.8 ms ($n = 7$; Fig. 8 B), further reflecting the rhythmicity (Budick and O'Malley, 2000; Buss and Drapeau, 2001, 2002; Ritter et al., 2001; Luna et al., 2004; Muller and Van Leeuwen, 2004; Masino and Fetcho, 2005). The compound currents that formed a plateau current represented a combination of primary EPCs and electrotonic reflections of EPCs generated in neighboring muscle (Fig. 8 C). These sequential primary EPCs represented either sequential firing of the same secondary motor neuron or asynchronous firing of different motor neurons.

Approximately 70% of the complex plateau responses analyzed were preceded by a slow rising component termed leading edge current (LEC) (Fig. 8 C and Fig. 9 A). This component represented a transjunctional reflection of evoked synaptic current generated in neighboring slow muscle. In the presence of 18βGA to block electrical coupling, the frequency of observed LECs decreased significantly along with the amplitude of the remaining LECs observed (Fig. 9). To ensure that the LEC was not a secondary consequence of the mutation in *relaxed*, we recorded LECs in wild-type fish that were treated with 1 M formamide to minimize contractions (Fig. 8 D). The average LEC amplitude recorded in wild-type fish (245 ±180 pA, $n = 53$) was similar to *relaxed* mutant fish (308 ± 220 pA, $n = 200$). Occasionally, during a fictive burst, rhythmic plateau currents lacking evidence of EPC components were observed. These simplified slow rising and decaying events

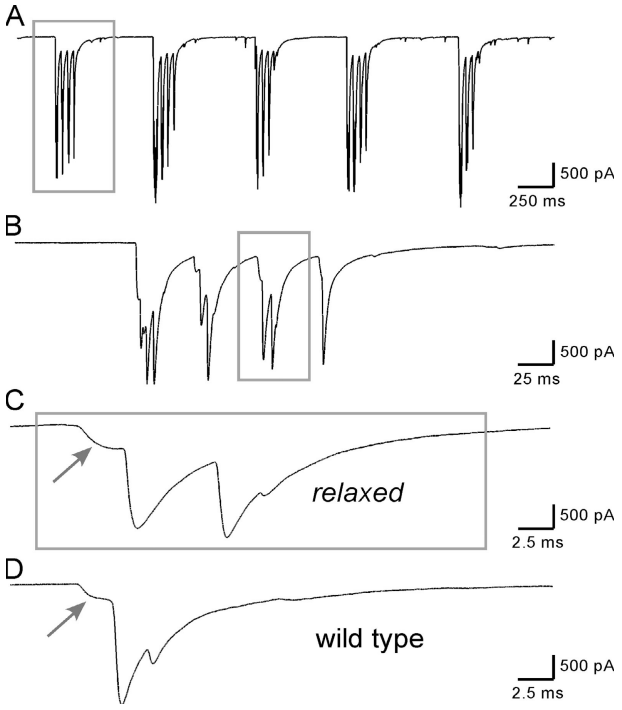

Figure 8. Slow muscle EPCs associated with photoactivated fictive swimming in the paralytic mutant line *relaxed*. (A) The rhythmic EPC pattern associated with beat and glide fictive swimming. Five separate swimming episodes with intervening glide segments were recorded from a slow muscle cell held at −90 mV. (B) A beat series is expanded to show the EPC patterns. (C) The asynchronous EPC pattern associated with a single tail beat. The leading edge current (LEC) is indicated by an arrow. (D) For comparison, an LEC from a wild-type fish treated with 1 M formamide to block contractions.

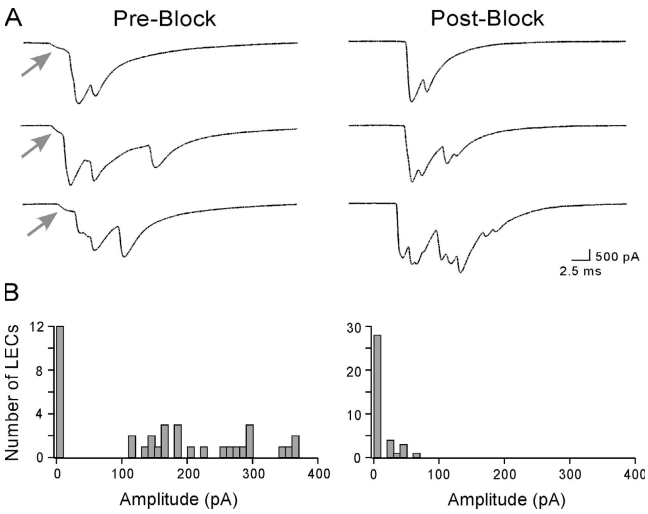

Figure 9. Effects of 18βGA on leading edge currents associated with fictive swimming. (A) The complex EPC pattern associated with a single rostral to caudal beat recorded from slow muscle during a fictive swimming bout. Examples of EPC bursts with LECs before (left) and after (right) treatment with 100 μM 18βGA. (B) Frequency histograms of LEC amplitude before (left) and after (right) addition of 18βGA. EPC bursts lacking LECs were scored as 0 amplitude.

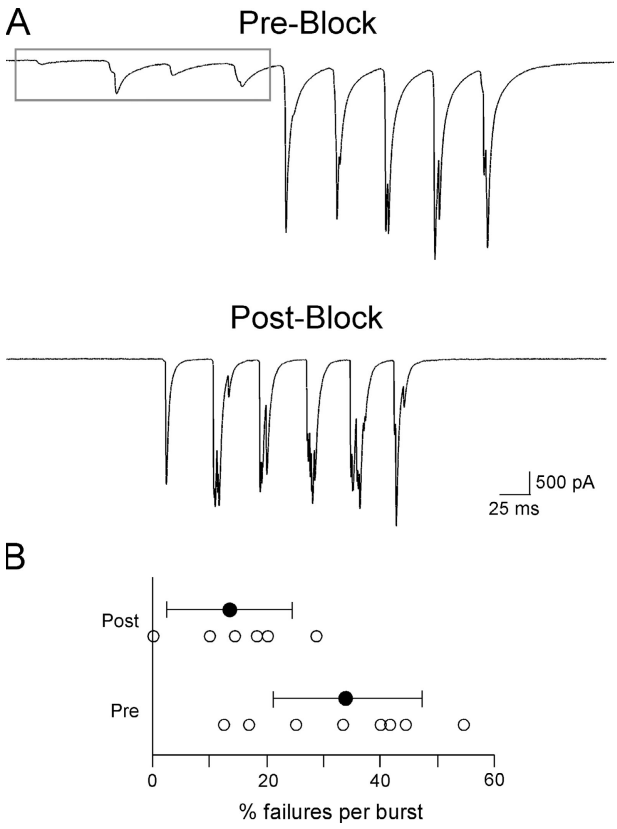

Figure 10. Fictive swimming in slow muscle reveals synaptic failures. (A) Intracellular recording from slow muscle during bouts of fictive rhythmic swimming before (top trace) and after (bottom trace) application of 100 μM 18βGA. Shown by boxed region are large EPCs that are preceded by a series of small inward currents that lack evidence of primary EPCs. (B) A frequency histogram of the fraction of failures per burst measured before and after 18βGA indicates that the number of electrotonic reflections of synaptic failures is reduced by blocking gap junctions.

resembled LECs in rise time and amplitude (Fig. 10 A). These similarities suggest that the simple plateau currents reflect failure of motor neuron excitation in this muscle cell so that only the transjunctional reflections were seen. Treatment with 18βGA (Fig. 10 A) reduced the average frequency of failure per burst from 34% to 13% (Fig. 10 B).

Paired slow muscle recordings support the idea that the LEC represents the transjunctional reflections of primary synaptic currents. When the recording electrodes were placed in adjacent segments, the LEC always appeared first in the more rostral segment (Fig. 11 A). The average intersegmental delay was 1.2 ± 0.6 ms (n = 6; Fig. 11 C), which corresponded well with the imposed delay that results from network filtering (1.3 ± 0.5 ms, n = 11; Fig. 6 D). This intersegmental delay in LEC onset also agrees with the intersegmental delay in contraction that accompanies rhythmic swimming (Budick and O'Malley, 2000; Ritter et al., 2001; Muller and Van Leeuwen, 2004). By contrast, when the paired electrodes were placed within the same segment, the average LEC delay was 0.3 ± 0.5 ms (n = 6; Fig. 11, B and C). This would be expected if both cells were simultaneously activated by their neighboring muscle contacts in the more rostral segment.

DISCUSSION

In most vertebrates, slow and fast skeletal muscle cells are interspersed, complicating muscle type–specific analysis of synaptic function (Hess, 1970; Morgan and Proske, 1984). However, in zebrafish tail, these muscle types can be readily identified on the basis of differences in position and orientation, thereby providing an unusual opportunity to compare their functional properties (van Raamsdonk et al., 1978, 1982; Buss and Drapeau, 2000; Luna et al., 2004). Fast and slow skeletal muscle in zebrafish serve different roles in motility, with the latter principally responsible for rhythmic swimming and the former controlling the powerful C-bend that sets in motion the escape response (Bone, 1978; Liu and Westerfield, 1988; Fetcho, 1987, 1992). Functionally, slow muscle in zebrafish is inexcitable and relies solely on local synapse-mediated depolarizations for contraction, while fast muscle is able to generate action potentials (Buckingham and Ali, 2004).

Both slow and fast skeletal muscle types exhibit electrical coupling, but the extent of functional coupling is very different. Traditional dye measurements are not useful for determining the size of functional networks because the distance of spread is dependent on time.

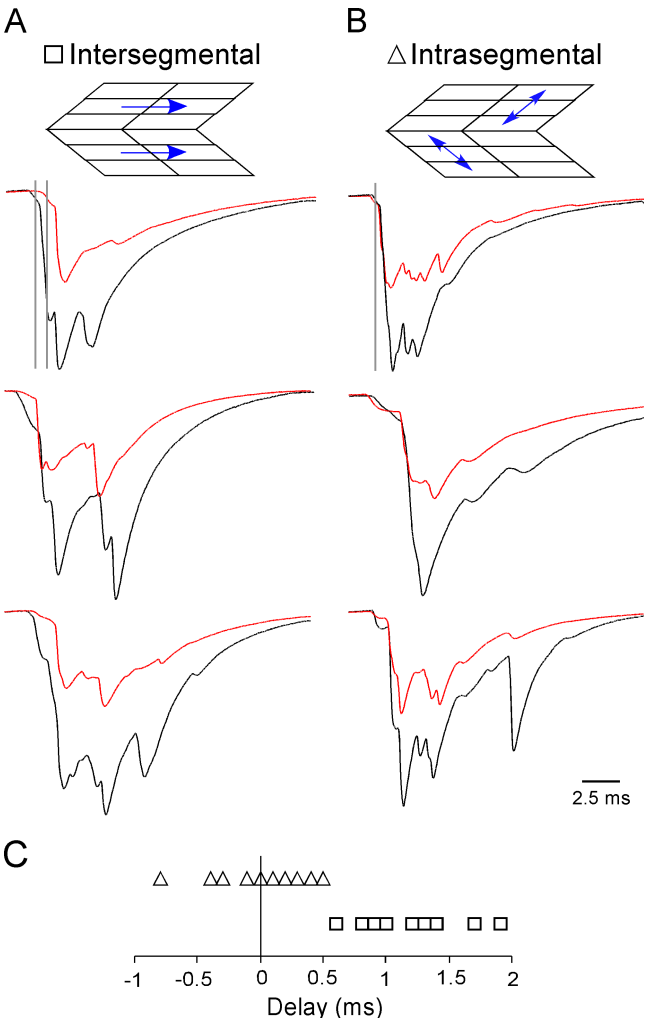

Figure 11. Intersegmental LEC delay reflects the network phase delay. (A) Three examples of paired intersegmental slow muscle recordings of single fictive swimming bouts. In all three examples, the rostral cell LEC (black) precedes the caudal cell LEC (red). For clarity, caudal cell currents were reduced to 50% of the peak rostral cell amplitude. (B) The onsets of LECs in paired intrasegmental slow muscle occur nearly simultaneously. (C) Frequency histogram of intersegmental (square) versus intrasegmental (triangle) LEC delays recorded between adjacent slow muscle cells. Delays were based on the amount of time required for each LEC to reach 100 pA.

However, our measurements of synaptic current provide estimates of the number of cells composing the network and indicate that functional sharing is much greater in slow muscle. In addition to determining the extent of functional coupling, spontaneous synaptic currents can be used to determine the likely route taken by each synaptic current. This is possible because each intercellular transit imposes a phase delay along with attenuation in amplitude and slowing of kinetics. Distortion of synaptic potentials by transit through electrically coupled skeletal muscle was first observed in muscle cells of regenerating salamander limbs (Dennis, 1975). More recently, synaptic potentials (Buss and Drapeau, 2000) and currents (Luna et al., 2004) were shown to be slowed and attenuated by transjunctional passage in the tail muscle of zebrafish. Our studies now show that the levels of coupling as well as the functional roles played by electrical coupling differ between muscle types in zebrafish. In fast muscle, a low coupling coefficient, along with very fast synaptic kinetics, greatly limits the ability of synaptic current to transit intercellular junctions. Consequently, the amplitude ratio versus phase delay relationship for paired mEPCs reflects a functional network limited to a single transjunctional passage. Because only three clusters of points were observed in fast muscle, the most parsimonious interpretation was that the events were generated in either of the two cells or a neighbor cell common to both. By contrast, the amplitude ratio versus phase delay relationships for paired mEPCs in slow muscle were more complex, and often as many as five or more distinct clusters were identified. The additional clusters were ascribed to transit through two cell boundaries on the basis of attenuation and kinetics. Because slow muscle forms a single layer and coupling is symmetrical, the two-dimensional network predicted by passage through two cells was shown to be composed of 12 surrounding muscle cells. This network feature, based on current relationships, was remarkably consistent with the directional spread of Lucifer yellow in slow muscle (Fig. 1 C and Fig. 4 B; see also Nguyen et al., 1999; Buss and Drapeau, 2000). Additional evidence for a large functional network in slow muscle was provided by block of electrical coupling, whereupon a large increase in amplitude of the primary current class was observed. This increase in current reflected the amount of current that was normally lost to the network through electrical coupling. A network of 10 synaptically connected slow muscle cells was determined on the basis of dividing the average increase by the average amplitude of secondary currents. Using yet another method of estimation, dividing the frequency of secondary events by the frequency of primary events, again yielded a coupled network composed of 13 slow muscle cells. Thus, three different methods of estimation all pointed to a single transjunctional passage for fast muscle and at least two passages for slow muscle.

Physiological roles for electrical coupling in slow muscle are suggested by in vivo recordings of fictive swimming in the paralytic mutant line, *relaxed* (Granato et al., 1996; Ono et al., 2001). On the basis of gating currents, intracellular calcium release, and caffeine sensitivity, a mutation in the dihydropyridine receptor was proposed several years ago as causal to the paralysis (Ono et al., 2001). Recent studies confirmed this proposal (Schredelseker et al., 2005; Zhou et al., 2006). Importantly, synaptic transmission appears normal in *relaxed* (Ono et al., 2001), permitting measurements of fictive swimming motor output without the complication

of movement or requirement of postsynaptic receptor blockers (Buss and Drapeau, 2002). Measurements of fictive swimming indicated that evoked currents, like spontaneous synaptic currents, were electrotonically distributed among cells of the slow muscle network (Buss and Drapeau, 2002; Luna et al., 2004). In the case of evoked currents, this sharing likely counteracted the large variability in synaptic current between cells that result from a low quantal content. A low quantal content and propensity for synaptic failure is seen in fast muscle (Wen and Brehm, 2005) and, as shown here, for slow muscle as well. An additional source of uneven distribution of synaptic depolarization of slow muscle was the asynchronous firing of motor neurons within segments. These differences in synaptic drive are likely not unique to developing zebrafish tail muscle cells. For example, in lampreys some muscle cells lack innervation and depend on synaptic responses from electrically coupled partner cells for depolarizing drive (Teravainen, 1971). At newly formed synapses of salamanders (Dennis, 1975) and rat embryos (Dennis et al., 1981), transmission is weak and electrical coupling has been proposed as a mechanism to distribute synaptic drive.

In the case of zebrafish slow muscle, the intrasegmental variability may be minimized by distributing synaptic current. This is achieved by means of coupling coefficients that were extremely high and with synaptic currents that exhibited fivefold slower kinetics than fast muscle. These slow currents were more effective at transjunctional passage and, following a single passage, the low pass filter further slowed kinetics for even more effective transit. The consequences of a distributed slow sustained current, in conjunction with asynchronous firing of motor neurons, resulted in a plateau current that ensured prolonged and effective depolarization (Fig. 8; see also Buss and Drapeau, 2002).

Intersegmental distribution of synaptic current may play an even more important role than intrasegmental distributions in rhythmic swimming. Consistent with a previously hypothesized role for electrical coupling (Buss and Drapeau, 2000), our fictive swimming recordings directly indicated a role of electrical coupling in the coordination of rhythmic swimming. Moreover, we have identified an intersegmental transjunctional reflection of evoked synaptic currents, termed leading edge current (LEC), which often preceded the active synaptic responses in that segment. This LEC was always a reflection of the more rostral segment endplate current and was blocked by inhibitors of electrical coupling. These LECs averaged ~15% of the primary EPC amplitude, which agreed reasonably well with our estimates of coupling coefficients for spontaneous synaptic currents. Previous paired recordings of fictive swimming may have failed to detect this LEC because the fish were partially curarized, which reduced the synaptic response amplitude and associated contractions (Buss and Drapeau, 2002). Importantly, intersegmental LECs were phase delayed by 1 to 2 ms with rostral always preceding caudal. This intersegmental delay corresponded well with the phase delay recorded for spontaneous synaptic currents in slow muscle. The intersegmental delay, imposed by low pass network filtering, reflected the driving force offered by inactive sink muscle cells in the adjacent caudal segment. On the basis of these data, we propose that the LECs are the mechanism through which the next segment is primed for the arrival of the signal from the nervous system. In this way, the propagation of contraction will be set to some degree by the fidelity of the low pass filter, which is likely to be more precise than the sequential firing of segmental motor neurons. This fixed intersegmental delay would help propagate the contractile wave at nearly uniform velocity along the length of the fish (Webb et al., 1984; Budick and O'Malley, 2000; Muller and Van Leeuwen, 2004).

The idea that electrical coupling plays a role in the temporal coordination of rhythmic activity has precedence in the central nervous system. For example, both olfactory bulb neurons (Schoppa and Westbrook, 2002; Christie et al., 2005) and cells of the inferior olive (Llinas et al., 1974; Devor and Yarom, 2002; Leznik and Llinas, 2005) require electrical coupling for correlated spiking. A role for electrical coupling and low pass filtering in the generation of rhythmic and synchronous activity has also been reported for subsets of GABA neurons of the neocortex (Galarreta and Hestrin, 1999; Gibson et al., 1999). In contrast, for zebrafish slow muscle, the properties of the low pass filtering would be used to distribute the depolarization in a precisely timed, but asynchronous, manner. This also contrasts sharply with fast muscle, which is weakly coupled and often completely uncoupled. Fast muscle controls fast fatiguing escape responses through fivefold faster synaptic kinetics and membrane excitability. Studies on a mutant zebrafish line that shows excessive electrical coupling in fast muscle illustrates the dire consequences when coupling is increased in this muscle type (Luna et al., 2004). Instead of eliciting a fast C-bend characteristic of the escape response, the fish is locked into a slow embryonic tail coil. Thus, our overall findings point to a previously unappreciated importance of electrical coupling in the regulation of skeletal muscle contraction, which is muscle type specific.

Thanks to Joe Fetcho, Peter Brink, and Fumihito Ono for insightful discussions.

This work was supported by a grant from the National Institutes of Health (NS 018205). V.M. Luna is a member of the Neuroscience graduate program.

Olaf S. Andersen served as editor.

Submitted: 31 January 2006
Accepted: 1 June 2006

REFERENCES

Armstrong, D.L., L. Turin, and A.E. Warner. 1983. Muscle activity and the loss of electrical coupling between striated muscle cells in *Xenopus* embryos. *J. Neurosci.* 3:1414–1421.

Bennett, M.V. 1966. Physiology of electrotonic junctions. *Ann. N. Y. Acad. Sci.* 137:509–539.

Blackshaw, S.E., and A.E. Warner. 1976. Low resistance junctions between mesoderm cells during development of trunk muscles. *J. Physiol.* 255:209–230.

Bone, Q. 1978. Locomotor muscle. *In* Fish Physiology. W.S. Hoar and D.J. Randall, editors. Academic Press, New York. 361–424.

Buckingham, S.D., and D.W. Ali. 2004. Sodium and potassium currents of larval zebrafish muscle fibres. *J. Exp. Biol.* 207:841–852.

Budick, S.A., and D.M. O'Malley. 2000. Locomotor repertoire of the larval zebrafish: swimming, turning and prey capture. *J. Exp. Biol.* 203:2565–2579.

Buss, R., and P. Drapeau. 2000. Physiological properties of zebrafish embryonic red and white muscle fibers during early development. *J. Neurophysiol.* 84:1545–1557.

Buss, R., and P. Drapeau. 2001. Synaptic drive to motoneurons during fictive swimming in the developing zebrafish. *J. Neurophysiol.* 86:197–210.

Buss, R., and P. Drapeau. 2002. Activation of embryonic red and white muscle fibers during fictive swimming in the developing zebrafish. *J. Neurophysiol.* 87:1244–1251.

Christie, J.M., C. Bark, S.G. Hormuzdi, I. Helbig, H. Monyer, and G.L. Westbrook. 2005. Connexin36 mediates spike synchrony in olfactory bulb glomeruli. *Neuron.* 46:761–772.

Constantin, B., and L. Cronier. 2000. Involvement of gap junctional communication in myogenesis. *Int. Rev. Cytol.* 196:1–65.

Davidson, J.S., I.M. Baumgarten, and E.H. Harley. 1986. Reversible inhibition of intercellular junctional communication by glycyrrhetinic acid. *Biochem. Biophys. Res. Commun.* 134:29–36.

Davidson, J.S., and I.M. Baumgarten. 1988. Glycyrrhetinic acid derivatives: a novel class of inhibitors of gap-junctional intercellular communication. Structure-activity relationships. *J. Pharmacol. Exp. Ther.* 246:1104–1107.

Dennis, M.J. 1975. Physiological properties of junctions between nerve and muscle developing during salamander limb regeneration. *J. Physiol.* 244:683–702.

Dennis, M.J., L. Ziskind-Conhaim, and A.J. Harris. 1981. Development of neuromuscular junctions in rat embryos. *Dev. Biol.* 81:266–279.

Devor, A., and Y. Yarom. 2002. Electrotonic coupling in the inferior olivary nucleus revealed by simultaneous double patch recordings. *J. Neurophysiol.* 87:3048–3058.

Fatt, P., and B. Katz. 1952. Spontaneous subthreshold activity at motor nerve endings. *J. Physiol.* 117:109–128.

Fetcho, J.R. 1987. A review of the organization and evolution of motoneurons innervating the axial musculature of vertebrates. *Brain Res.* 434:243–280.

Fetcho, J.R. 1992. The spinal motor system in early vertebrates and some of its evolutionary changes. *Brain Behav. Evol.* 40:82–97.

Galarreta, M., and S. Hestrin. 1999. A network of fast-spiking cells in the neocortex connected by electrical synapses. *Nature.* 402:72–75.

Gibson, J.R., M. Beierlein, and B.W. Connors. 1999. Two networks of electrically coupled inhibitory neurons in neocortex. *Nature.* 402:75–79.

Goldberg, G.S., A.P. Moreno, J.F. Bechberger, S.S. Hearn, R.R. Shivers, D.J. MacPhee, Y.C. Zhang, and C.C. Naus. 1996. Evidence that disruption of connexon particle arrangements in gap junction plaques is associated with inhibition of gap junctional communication by a glycyrrhetinic acid derivative. *Exp. Cell Res.* 222:48–53.

Granato, M., F. van Eeden, U. Schach, T. Trowe, M. Brand, M. Furutani-Seiki, P. Haffter, M. Hammerschmidt, C. Heisenberg, Y. Jiang, et al. 1996. Genes controlling and mediating locomotion behavior of the zebrafish embryo and larva. *Development.* 123:399–413.

Hess, A. 1970. Vertebrate slow muscle fibers. *Physiol. Rev.* 50:40–62.

Jaramillo, F., S. Vicini, and S.M. Schuetze. 1988. Embryonic acetylcholine receptors guarantee spontaneous contractions in rat developing muscle. *Nature.* 335:66–68.

Leznik, E., and R. Llinas. 2005. Role of gap junctions in synchronized neuronal oscillations in the inferior olive. *J. Neurophysiol.* 94:2447–2456.

Liu, D.W., and M. Westerfield. 1988. Function of identified motoneurones and co-ordination of primary and secondary motor systems during zebra fish swimming. *J. Physiol.* 403:73–89.

Llinas, R., R. Baker, and C. Sotelo. 1974. Electrotonic coupling between neurons in cat inferior olive. *J. Neurophysiol.* 37:560–571.

Luna, V.M., M. Wang, F. Ono, M.R. Gleason, J.E. Dallman, G. Mandel, and P. Brehm. 2004. Persistent electrical coupling and locomotory dysfunction in the zebrafish mutant shocked. *J. Neurophysiol.* 92:2003–2009.

Masino, M., and J.R. Fetcho. 2005. Fictive swimming motor patterns in wild type and mutant larval zebrafish. *J. Neurophysiol.* 93:3177–3188.

Morgan, D.L., and U. Proske. 1984. Vertebrate slow muscle: its structure, pattern of innervation, and mechanical properties. *Physiol. Rev.* 64:103–169.

Muller, U.K., and J.L. Van Leeuwen. 2004. Swimming of larval zebrafish: ontogeny of body waves and implications for locomotory development. *J. Exp. Biol.* 207:853–868.

Nguyen, P.V., L. Aniksztejn, S. Catarsi, and P. Drapeau. 1999. Maturation of neuromuscular transmission during early development in zebrafish. *J. Neurophysiol.* 81:2852–2861.

Ono, F., S. Higashijima, A. Shcherbatko, J.R. Fetcho, and P. Brehm. 2001. Paralytic zebrafish lacking acetylcholine receptors fail to localize rapsyn clusters to the synapse. *J. Neurosci.* 21:5439–5448.

Proulx, A., P. Merrifield, and C. Naus. 1997. Blocking gap junctional intercellular communication in myoblasts inhibits myogenin and MRF4 expression. *Dev. Genet.* 20:133–144.

Ritter, D.A., D.H. Bhatt, and J.R. Fetcho. 2001. In vivo imaging of zebrafish reveals differences in the spinal networks for escape and swimming movements. *J. Neurosci.* 21:8956–8965.

Saez, J.C., V.M. Berthoud, M.C. Branes, A.D. Martinez, and E.C. Beyer. 2003. Plasma membrane channels formed by connexins. *Physiol. Rev.* 83:1359–1400.

Schmalbruch, H. 1982. Skeletal muscle fibers of newborn rats are coupled by gap junctions. *Dev. Biol.* 91:485–490.

Schoppa, N.E., and G.L. Westbrook. 2002. AMPA autoreceptors drive correlated spiking in olfactory bulb glomeruli. *Nat. Neurosci.* 5:1194–1202.

Schredelseker, J., V. Di Biase, G.J. Obermair, E.T. Felder, B.E. Flucher, C. Franzini-Armstrong, and M. Grabner. 2005. The beta1a subunit is essential for the assembly of dihydropyridine-receptor arrays in skeletal muscle. *Proc. Natl. Acad. Sci. USA.* 102:17219–17224.

Teravainen, H. 1971. Anatomical and physiological studies on muscles of lamprey. *J. Neurophysiol.* 34:954–973.

Van der Kloot, W., and L.A. Naves. 1996. Localizing quantal currents along frog neuromuscular junctions. *J. Physiol.* 497:189–198.

van Raamsdonk, W., C.W. Pool, and G. Te Kronnie. 1978. Differentiation of muscle fiber types in the teleost *Brachydanio rerio*. *Anat. Embryol. (Berl.)*. 153:137–155.

van Raamsdonk, W., L. van't Veer, K. Veeken, C. Heyting, and C.W. Pool. 1982. Differentiation of muscle fiber types in the teleost *Brachydanio rerio,* the zebrafish. *Anat. Embryol. (Berl.)*. 164:51–62.

Webb, P.W., P.T. Kostecki, and E. Stevens. 1984. The effect of size and swimming speed on locomotor kinematics of rainbow trout. *J. Exp. Biol*. 109:77–95.

Wen, H., and P. Brehm. 2005. Paired motor neuron-muscle recordings in zebrafish test the receptor blockade model for shaping synaptic current. *J. Neurosci*. 25:8104–8111.

Wernig, A. 1976. Localization of active sites in the neuromuscular junction of the frog. *Brain Res*. 118:63–72.

Zhou, W., L. Saint-Amant, H. Hirata, W.W. Cui, S.M. Sprague, and J.Y. Kuwada. 2006. Non-sense mutations in the dihydropyridine receptor beta1 gene, CACNB1, paralyze zebrafish relaxed mutants. *Cell Calcium*. 39:227–236.